

# Potential for measuring the $H^\pm W^\mp Z^0$ vertex from $WZ$ fusion at the Large Hadron Collider

Eri Asakawa,<sup>1,\*</sup> Shinya Kanemura,<sup>2,†</sup> and Junichi Kanzaki<sup>3,‡</sup>

<sup>1</sup>*Theory Group, KEK,*

*Tsukuba, Ibaraki 305-0801, Japan*

<sup>2</sup>*Department of Physics, University of Toyama,  
3190 Gofuku, Toyama 930-8555, Japan*

<sup>3</sup>*Institute of Particle and Nuclear Studies, KEK,  
Tsukuba, Ibaraki 305-0801, Japan*

## Abstract

We investigate the possibility of measuring the  $H^\pm W^\mp Z^0$  vertex from the single  $H^\pm$  production process via  $WZ$  fusion at the CERN Large Hadron Collider (LHC). This vertex strongly depends on the structure of the Higgs sector in various new physics scenarios, so that its measurement can be useful to distinguish the models. A signal and background simulation under the expected detector performance at LHC is done for the decay modes of  $H^\pm \rightarrow t\bar{b}(\bar{t}b)$  and  $H^\pm \rightarrow W^\pm Z^0$ , and the required magnitudes of the vertex for observation are evaluated. It is found that this process with the decay  $H^\pm \rightarrow W^\pm Z^0$  can be useful to test the model with a real and a complex triplets where the  $H^\pm W^\mp Z^0$  vertex appears at the tree level, while the loop induced  $H^\pm W^\pm Z^0$  vertex in multi-Higgs doublet models cannot be measurable via the decay mode of  $H^\pm \rightarrow t\bar{b}(\bar{t}b)$ .

PACS numbers: 12.60.Fr, 14.80.Cp

Keywords: Higgs, LHC, Beyond the Standard Model

---

\*Electronic address: eri@post.kek.jp

†Electronic address: kanemu@sci.u-toyama.ac.jp

‡Electronic address: Junichi.Kanzaki@cern.ch

## I. INTRODUCTION

The idea of spontaneous breaking of the electroweak gauge symmetry will soon be tested directly at the CERN Large Hadron Collider (LHC) [1]. There, it is expected that a Higgs boson of the standard model (SM) can be detected in a wide range of the mass, which is the last unknown parameter of the model. On the other hand, it is possible that the structure of the Higgs sector takes a non-minimal form with additional isospin-singlets, doublets, triplets etc. Indeed, there is a variety of new physics scenarios which deduce extended Higgs sectors in the low energy effective theory. Therefore, the experimental determination of the structure of the Higgs sector is essentially important to select new physics beyond the SM.

Current precision data provide important hints for the structure of the Higgs sector. In particular, all the Higgs models must respect the experimental fact that the electroweak rho parameter ( $\rho$ ) is very close to unity. It is well known that the tree-level prediction of  $\rho = 1$  is a common feature of Higgs models with only doublets (and singlets). On the other hand, the rho parameter data give a strong constraint on the models which additionally include triplets or greater representations of the isospin  $SU(2)$  gauge symmetry, because in these cases the predicted rho parameter is generally not unity already at the tree level [2]. There are two simple possibilities to satisfy this constraint. First, these multiplets but doublets do not contribute to the electroweak spontaneous symmetry breaking much, and their vacuum expectation values are sufficiently small as compared to those of doublets. Second, we can consider models arranging the custodial  $SU(2)$  symmetry among these additional multiplets, so that the models then naturally impose  $\rho = 1$  at the tree level [3, 4, 5, 6]. The Left-Right symmetric model [7], the Littlest Higgs model [8, 9] and some extra dimension models [10] predict an additional complex triplet as well. In order to determine the structure of extended Higgs model, it is important to discriminate these models that satisfy  $\rho \simeq 1$  at future collider experiments.

In extended Higgs models, additional Higgs bosons like charged and CP-odd scalar bosons are predicted. Phenomenology of these extra scalar bosons strongly depends on the characteristics of each new physics model. By measuring their properties like masses, widths, production rates and decay branching ratios, the outline of the physics beyond the electroweak scale can be experimentally determined. The coupling of singly-charged Higgs bosons with the weak gauge bosons,  $H^\pm W^\mp Z^0$ , is of particular importance for such an

approach[11, 12, 13, 14, 15, 16]. The vertex is expressed by

$$i\Gamma_{H^\pm W^\mp Z}(p_W, p_Z; \lambda_W, \lambda_Z) = igm_W V_{\mu\nu} \epsilon_W^{*\mu}(p_W, \lambda_W) \epsilon_Z^{*\nu}(p_Z, \lambda_Z), \quad (1)$$

where  $g$  is the weak gauge coupling,  $m_W$  is the mass of the weak boson  $W^\pm$ , and  $\epsilon_V^{*\mu}(p_V, \lambda_V)$  ( $V = W$  and  $Z$ ) are polarization vectors for the outgoing weak gauge bosons with the momentum  $p_V$  and the helicity  $\lambda_V$ . Here,  $V_{\mu\nu}$  is decomposed in terms of three form factors as

$$V_{\mu\nu} = F g_{\mu\nu} + \frac{G}{m_W^2} p_{Z\mu} p_{W\nu} + \frac{H}{m_W^2} \epsilon_{\mu\nu\rho\sigma} p_Z^\rho p_W^\sigma, \quad (2)$$

where the antisymmetric tensor  $\epsilon_{\mu\nu\rho\sigma}$  is defined so as to satisfy  $\epsilon_{0123} = -1$ . The values of  $F$ ,  $G$  and  $H$  depend on the detail of the model. The leading contribution is well described by  $F$ , and its magnitude is directly related to the structure of the extended Higgs sector under global symmetries[2, 11]. It can appear at the tree level in models with scalar triplets, while it is induced at the loop level in multi scalar doublet models. In Ref. [16], the new physics predictions to the  $H^\pm W^\mp Z^0$  are summarized and possible size of the signal cross section in each model is evaluated.

In this paper, we consider testing the  $H^\pm W^\mp Z^0$  coupling via the single charged Higgs boson production in the  $WZ$  fusion process at the LHC. Higgs production processes via vector boson fusion (VBF) have an advantage over the other production processes, because the signal can be completely reconstructed and produced jets are suppressed in the central region due to a lack of color flow between the initial state quarks. A signal and background simulation under the expected detector performance at LHC is performed for the decay modes  $H^\pm \rightarrow t\bar{b}(\bar{t}b)$  and  $H^\pm \rightarrow W^\pm Z^0$ . We estimate the minimum value of the form factor  $|F|^2$  above which the signal significance can be substantial for a possibility of detection at the LHC. We then discuss which new physics models can be tested via these processes.

## II. SIGNAL AND BACKGROUNDS

### A. Charged Higgs production via vector boson fusion

VBF is a pure electroweak process without color flow in the central region. The process naturally leads to high transverse momentum ( $P_T$ ) tag jets in the forward region and allow to observe small hadronic activity in the central region except for jets from produced Higgs

boson. Hence it is possible to observe small electroweak signal rates in a region of phase space not very populated by QCD background events. Such an advantage of VBF has been used for neutral Higgs boson production for intermediate and greater masses of Higgs bosons [1, 17, 18, 19, 20]. This can also be applied for charged Higgs boson production from  $WZ$  fusion, which we discuss in this paper.

In Fig. 1, the hadronic cross section of  $pp \rightarrow W^{\pm*}Z^0 X \rightarrow H^{\pm}X$  at the LHC ( $\sqrt{s} = 14$  TeV) is shown as a function of mass  $m_{H^{\pm}}$  of the charged Higgs boson [16]. The form factors  $F$ ,  $G$  and  $H$  of the  $H^{\pm}W^{\mp}Z^0$  vertex are set to be 1, 0 and 0, respectively. The magnitude of  $\sigma^{|F|^2=1}$  can be about 3900 fb for  $m_{H^{\pm}} = 200$  GeV, 470 fb for  $m_{H^{\pm}} = 500$  GeV, 210 fb for  $m_{H^{\pm}} = 700$  GeV and 150 fb for  $m_{H^{\pm}} = 800$  GeV. The prediction of the cross section in each new physics scenario can be obtained by rescaling the value of  $F$ . The typical values of  $F$  in several models are summarized in Ref. [16].

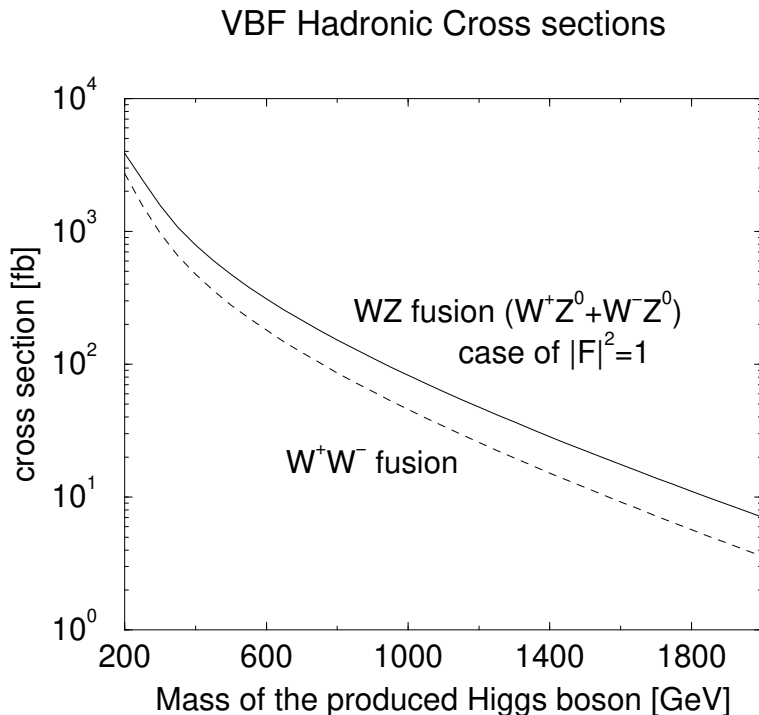


FIG. 1: The hadronic cross section of the  $W^{\pm}Z^0$  fusion process and the  $W^+W^-$  fusion process as a function of the mass of the charged and neutral Higgs bosons, respectively. For the  $W^{\pm}Z^0$  fusion, the form factor  $F$  is set to be unity. The SM prediction is shown for the  $W^+W^-$  fusion.

## B. Event selection

### 1. Higgs production via VBF

#### Forward jet tagging

A characteristic of VBF is that the colliding quarks are scattered with relatively high  $P_T$ . These scattered partons can easily be identified as jets in forward region of the detector. Since the two forward jets  $j_1$  and  $j_2$  lie in opposite hemispheres with large pseudo-rapidity separation between them, we can impose the cut

$$\Delta\eta_{j_1j_2} \equiv |\eta_{j_1} - \eta_{j_2}| > 2 - 4, \quad (3)$$

where the cut value is adjusted depending on the Higgs mass and decay modes so as to make it most effectively. With this cut, QCD backgrounds are typically suppressed by a few orders of magnitude, while the signal rate is suppressed at most by a factor of 2–3. We also impose the constraints for the invariant mass of two forward jets, whose physical meaning is similar to that in the constraint in Eq. (3);

$$M_{j_1j_2} > 500 - 1000\text{GeV}. \quad (4)$$

#### Central jet veto

Since VBF is a pure electroweak process without color flow in the central region, it allows to observe small hadronic activity except for jets which are the tagging jets and the decay products from produced Higgs boson. We then impose the veto on the additional production of jets in the central region (between two tagging jets).

### 2. Higgs decay

Here we consider the kinematic cuts of the  $t\bar{b}$  ( $\bar{t}b$ ) decay mode and the  $W^\pm Z^0$  decay mode separately. We impose the basic cuts for the invariant mass, and those for the number of jets,  $b$ -jets and leptons which should be the appropriate number for each final state. In order to improve the significance  $S/\sqrt{B}$ , we impose further several effective cuts which we explain below.

#### The $t\bar{b}$ ( $\bar{t}b$ ) decay mode

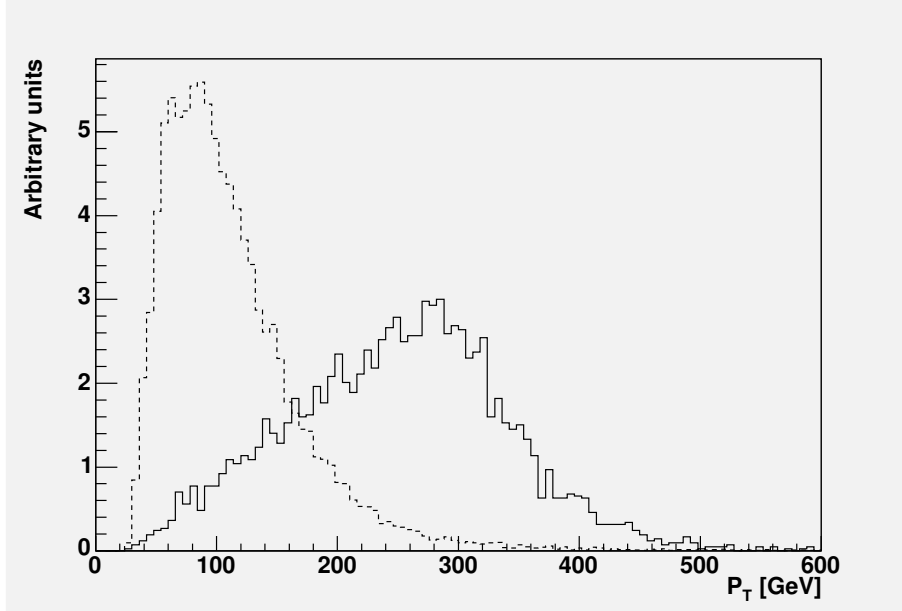


FIG. 2: The  $P_T$  distribution for the  $b$ -jets with the highest  $P_T$  from the signal ( $H^\pm \rightarrow t\bar{b}$  ( $\bar{t}b$ ) modes at  $m_H^\pm = 700$  GeV) and background (top pair production). Solid (dashed) histogram represents the signal (top pair production).

The final state  $2b + \ell + \cancel{E}_T$  with two tagging jets is studied here. The main background is the top pair production whose cross section amounts to about 490 pb.

For the  $H^- \rightarrow \bar{t}b$  mode, one  $b$ -jet ( $b$ ) comes directly from the  $H^-$  decay, and the other  $b$ -jet ( $\bar{b}$ ) does from the decay of the top quark which is a decay product of  $H^-$ . For  $H^-$  with a relatively large mass, the former  $b$ -jet tends to have higher  $P_T$  than the  $b$ -jet from the top quark decay. Then, the cut for the  $b$ -jet with higher  $P_T$  is helpful for reducing the top pair production events. The same happens for the  $H^+ \rightarrow t\bar{b}$  mode (Fig. 2).

### The $W^\pm Z^0$ decay mode

For the model with a real and a complex triplet fields [3, 4, 5], the  $H^\pm \rightarrow W^\pm Z^0$  decay mode is dominant because  $H^\pm$  do not couple to fermions. We consider the sequential decay mode  $W^\pm \rightarrow \ell^\pm \nu$  and  $Z \rightarrow jj$  or  $\ell\ell$ , that is, the final states are the  $2j + \ell + \cancel{E}_T$  and  $3\ell + \cancel{E}_T$  with two tagging jets. For both the cases, the most serious background comes from the  $W + 4jets$  events. Even after the forward jet tagging ( $\Delta\eta_{j_1 j_2} > 2.5$  and  $M_{j_1 j_2} > 500$  GeV), the cross section exceeds 130 pb. Though the top pair production is also the serious background, eliminating the events which have two  $b$ -jets drastically reduces the background

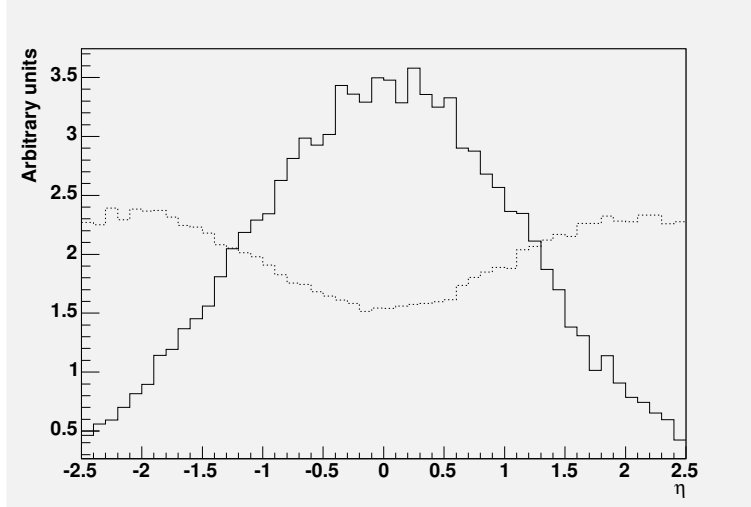


FIG. 3: The distribution for the pseudo-rapidity  $\eta$  of electrons from the signal ( $H^\pm \rightarrow W^\pm Z^0$  modes at  $m_H^\pm = 800$  GeV) and backgrounds (top pair production,  $W + 4j$ ). Solid (dotted) histogram represents the signal ( $W + 4j$ ).

from the top pair production [19].

Since the  $W + 4jets$  events are dominated by single  $W$  boson production processes  $u\bar{d}(\bar{u}d) \rightarrow W^\pm$  at the parton level, the helicities of the produced  $W$  bosons do not have the helicity 0 component. Then, the leptons coming from the  $W$  bosons are populated in the forward and backward direction, according to  $|\mathcal{M}(W^\pm \rightarrow \ell^\pm \nu)|^2 \sim |1 \pm \cos \theta|^2$ , where  $\theta$  is the scattering angle in the center-of-mass frame. On the other hand,  $W$  bosons coming from the  $H^\pm$  bosons are not polarized. Then, if we put a cut for the lepton direction, such as  $\eta_\ell < 1$  where  $\eta_\ell$  is the pseudo-rapidity of the lepton, a large amount of backgrounds can be effectively reduced (Fig. 3).

When  $H^\pm$  has relatively large masses, the produced  $W$  and  $Z$  bosons have large momenta and the trajectories of their decay products follow directions of their parent  $W$  and  $Z$  bosons approximately. Therefore, if the jets in the central region are labeled as  $j_3$  and  $j_4$ , and if the quantities  $\Delta R_{min} = \min(\Delta R_{\ell j_3}, \Delta R_{\ell j_4})$  and  $\Delta R_{max} = \max(\Delta R_{\ell j_3}, \Delta R_{\ell j_4})$  are defined, where  $\Delta R \equiv \sqrt{|\Delta\phi|^2 + |\Delta\eta|^2}$ , the relation  $\Delta R_{min} \simeq \Delta R_{max}$  is obtained for the signal process. On the other hand, the background processes do not necessarily satisfy this relation (Fig. 4 and Fig. 5). In addition, the jet-jet separation  $\Delta R_{j_3 j_4}$  has small value for the signal process (Fig. 6), so that we impose the cut  $\Delta R_{j_3 j_4} < 1$ .

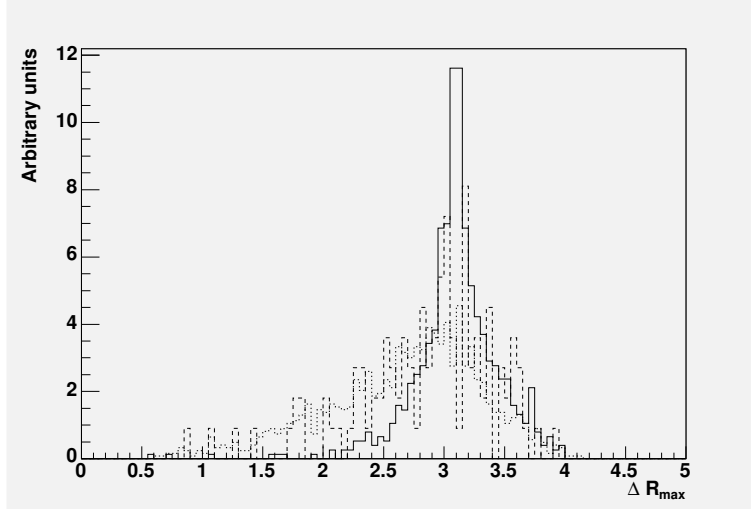


FIG. 4: The distribution for  $\Delta R_{max}$  from the signal ( $H^\pm \rightarrow W^\pm Z^0$  modes at  $m_H^\pm = 800$  GeV) and backgrounds (top pair production,  $W + 4j$ ). Solid (dashed, dotted) histogram represents the signal (top pair production,  $W + 4j$ ).

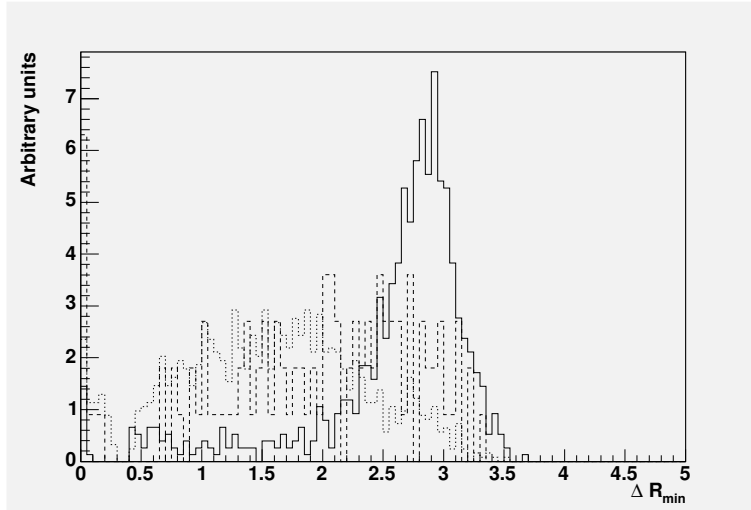


FIG. 5: The distribution for  $\Delta R_{min}$  from the signal ( $H^\pm \rightarrow W^\pm Z^0$  modes at  $m_H^\pm = 800$  GeV) and backgrounds (top pair production,  $W + 4j$ ). Solid (dashed, dotted) histogram represents the signal (top pair production,  $W + 4j$ ).

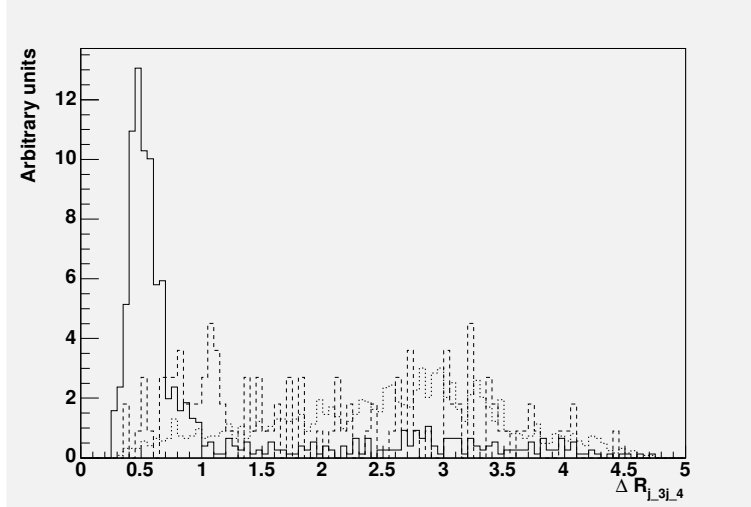


FIG. 6: The distribution for  $\Delta R_{j_3j_4}$  from the signal ( $H^\pm \rightarrow W^\pm Z^0$  modes at  $m_H^\pm = 800$  GeV) and backgrounds (top pair production,  $W + 4j$ ). Solid (dashed, dotted) histogram represents the signal (top pair production,  $W + 4j$ ).

### C. Results

The event generation for the processes except for  $W^\pm Z^0 jj$  production is performed by PYTHIA 6.2 [21].<sup>1</sup> We use the CTEQ5L parametrization [22] of the parton distribution functions. For the  $W^\pm Z^0 jj$  production, we use MadGraph [23] where the CTEQ6L [24] is adopted for the parton distribution function. In our study, we assume the branching ratio of the charged Higgs decay into each mode is 100% in order to give results in a model-independent way. When a particular model is considered, we have to multiply the branching ratios properly. For the detector performance we applied acceptance cuts and included smearing effects according to the ATLAS detector[25]. For  $W + 4j$  events, the events with  $M_{j_1j_2} > 500$  GeV and  $\Delta\eta_{j_1j_2} > 2.5$  are used in our simulation study.

#### 1. The $H^\pm \rightarrow t\bar{b}(\bar{t}b)$ decay mode

$$\underline{H^\pm \rightarrow t\bar{b}(\bar{t}b) \rightarrow bb\ell\nu}$$

<sup>1</sup> We use the neutral Higgs boson production process via VBF as a signal process. In order to deal with the process of charged Higgs boson production we compel the produced neutral Higgs bosons to decay into  $t\bar{b}$  ( $\bar{t}b$ ) or  $W^\pm Z^0$  in the generation.

The results of the efficiency for selection cuts are listed in Table I and II for  $m_{H^\pm} = 200$  and 700 GeV, respectively. The cuts applied in this analysis are:

- Forward jet tagging:

At least one jet in both forward ( $\eta \geq 0$ ) and backward ( $\eta < 0$ ) regions with  $P_T > 25$  GeV.

By defining a jet with the highest  $P_T$  in the forward (backward) region as  $j_1$  ( $j_2$ ),

$$\Delta\eta_{j_1 j_2} > 3.8, M_{j_1 j_2} > 550 \text{ GeV for } m_{H^\pm} = 200 \text{ GeV,}$$

$$\Delta\eta_{j_1 j_2} > 3.5, M_{j_1 j_2} > 800 \text{ GeV for } m_{H^\pm} = 700 \text{ GeV.}$$

- Lepton cuts:

One lepton with  $P_T > 30$  GeV.

- $b$ -jet cuts:

Two  $b$ -jets with  $P_T > 25$  GeV.

( $P_T$  of one  $b$ -jet with higher  $P_T$ )  $> 250$  GeV for  $m_{H^\pm} = 700$  GeV.

- Central jet veto:

No jet with  $P_T > 20$  GeV and  $\Delta R > 0.7$  from tag jets.

- invariant mass cuts:

$$M_{bb\nu} < 220 \text{ GeV for } m_{H^\pm} = 200 \text{ GeV.}$$

After these cuts are imposed, the signal events decrease to 0.32% (1.1%) for  $m_{H^\pm} = 200$  GeV (700 GeV), while a large reduction by about 2 orders (3 orders) of magnitude is observed in the background processes. Since the cross section for the top pair production is 490 pb, the signal cross sections of 160 fb and 22 fb are required to satisfy the statistical significance  $S/\sqrt{B} > 3$  for  $m_{H^\pm} = 200$  and 700 GeV, respectively, assuming the integrated luminosity as  $\mathcal{L} = 600 \text{ fb}^{-1}$ .

## 2. The $H^\pm \rightarrow W^\pm Z^0$ decay mode

$$\underline{H^\pm \rightarrow W^\pm Z^0 \rightarrow jj\ell\nu}$$

Efficiencies for the selection cuts are listed in Table III, IV and V for  $m_{H^\pm} = 200, 500$  and 800 GeV, respectively. The cuts applied in this analysis are:

	signal	background $t\bar{t}$
Before cuts	100% (160 fb)	100% (490 pb)
+Forward jet tagging	29% (46 fb)	4.1% (20 pb)
+Lepton cuts	4.1% (6.6 fb)	0.81% (4.0 pb)
+ $b$ -jet cuts	1.0% (1.6 fb)	0.42% (2.1 pb)
+Central jet veto	0.66% (1.1 fb)	0.060% (0.29 pb)
+invariant mass cuts	0.32% (0.51 fb)	0.0036% (18 fb)

TABLE I: Efficiencies and cross sections for the signal ( $H^\pm \rightarrow t\bar{b}(\bar{t}b)$  decay modes at  $m_H^\pm = 200$  GeV) and the background (top pair production). The cross sections are shown in parenthesis. For the signal, we show the cross sections which give  $S/\sqrt{B} \simeq 3$  for  $|F|^2 = 1$ .

	signal	background $t\bar{t}$
Before cuts	100% (22 fb)	100% (490 pb)
+Forward jet tagging	32% (7.0 fb)	2.1% (10.0 pb)
+Lepton cuts	5.5% (1.2 fb)	0.42% (2.1 pb)
+ $b$ -jet cuts	2.1% (0.46 fb)	0.0065% (0.032 pb)
+Central jet veto	1.1% (0.24 fb)	0.00079% (3.9 fb)

TABLE II: Efficiencies and cross sections for the signal ( $m_H^\pm = 700$  GeV) and the background (top pair production) for  $H^\pm \rightarrow t\bar{b}(\bar{t}b)$  decay mode. The cross sections are shown in parenthesis. For the signal, we show the cross sections which give  $S/\sqrt{B} \simeq 3$  for  $|F|^2 = 1$ .

- Forward jet tagging:

At least one jet in both forward ( $\eta \geq 0$ ) and backward ( $\eta < 0$ ) regions with  $P_T > 40$  GeV.

By defining a jet with the highest  $P_T$  in the forward (backward) region as  $j_1$  ( $j_2$ ),

$$\Delta\eta_{j_1 j_2} > 2.5, M_{j_1 j_2} > 500 \text{ GeV}.$$

- $b$ -jet cuts:

No  $b$ -jet with  $P_T > 25$  GeV.

- Lepton cuts:

One lepton with  $P_T > 30$  GeV and no other lepton with  $P_T > 20$  GeV,

$$(M_{\ell\nu})_T < 100 \text{ GeV},$$

$$\eta_\ell < 1.0.$$

- Central jet veto:

Two jets with  $P_T > 20$  GeV in the central region ( $\eta < 2.0$ ).

- Central jet cuts:

( $P_T$  of one central jet with higher  $P_T$ )  $> 50$  GeV for  $m_{H^\pm} = 200$  GeV,

( $P_T$  of one central jet with higher  $P_T$ )  $> 100$  GeV for  $m_{H^\pm} = 500, 700$  GeV,

$\Delta R_{j_3 j_4} < 1.0$  and  $\Delta R_{max} > 2.5$  for  $m_{H^\pm} = 500$  GeV,

$\Delta R_{j_3 j_4} < 1.0$ ,  $\Delta R_{min} > 2.5$  for  $m_{H^\pm} = 800$  GeV,

$60 \text{ GeV} < M_{j_3 j_4} < 100 \text{ GeV}$ .

The event selection also works effectively in order to reduce the  $WZ$  production whose cross section is 26 pb. According to our simulation study, the number of remaining events for the  $WZ$  and  $WZjj$  production processes is less than the one for  $W + 4jet$  production by at least 2 orders.

Since the cross section for the  $W + 4jet$  production (the top pair production) is about 130 pb (490 pb), the signal cross sections of 870 fb, 130 fb and 48 fb are required to satisfy  $S/\sqrt{B} > 3$  for  $m_{H^\pm} = 200, 500$  and 800 GeV, respectively, under  $\mathcal{L} = 600 \text{ fb}^{-1}$ .

$$\underline{H^\pm \rightarrow W^\pm Z^0 \rightarrow \ell\ell\nu}$$

Efficiencies for the selection cuts are listed in Table VI, VII and VIII for  $m_{H^\pm} = 200, 500$  and 800 GeV, respectively. The cuts applied in this analysis are:

- Forward jet tagging:

At least one jet in both forward ( $\eta \geq 0$ ) and backward ( $\eta < 0$ ) regions with  $P_T > 40$  GeV.

By defining a jet with the highest  $P_T$  in the forward (backward) region as  $j_1$  ( $j_2$ ),

$$\Delta\eta_{j_1 j_2} > 2.5, M_{j_1 j_2} > 500 \text{ GeV}.$$

	signal	backgrounds	
		$W + 4j$	$t\bar{t}$
Before cuts	100% (870 fb)	100% (130 pb)	100% (490 pb)
+Forward jet tagging	31% (270 fb)	50% (65 pb)	3.6% (18 pb)
+ $b$ -jet cuts	26% (230 fb)	47% (61 pb)	0.25% (1.2 pb)
+Lepton cuts	1.3% (11 fb)	2.0% (2.6 pb)	0.012% (0.059 pb)
+Central jet veto	0.39% (3.4 fb)	0.32% (0.42 pb)	0.0033% (0.016 pb)
+Central jet cuts	0.11% (0.96 fb)	0.043% (56 fb)	0.00079% (3.9 fb)

	backgrounds		
	$W^+ Z^0 jj$	$W^- Z^0 jj$	$WZ$
Before cuts	100% (350 fb)	100% (210 fb)	100% (26 pb)
+Forward jet tagging	43% (150 fb)	36% (76 fb)	1.1% (0.29 pb)
+ $b$ -jet cuts	37% (130 fb)	30% (63 fb)	0.99% (0.26 pb)
+Lepton cuts	1.5% (5.3 fb)	1.2% (2.5 fb)	0.015% (0.0039 pb)
+Central jet veto	0.40% (1.4 fb)	0.30% (0.63 fb)	0.0031% (0.81 fb)
+Central jet cuts	0.081% (0.28 fb)	0.072% (0.15 fb)	0.0006% (0.16 fb)

TABLE III: Efficiencies and cross sections for the signal ( $H^\pm \rightarrow W^\pm Z^0 \rightarrow jj\ell\nu$  decay modes at  $m_H^\pm = 200$  GeV) and backgrounds ( $W + 4j$ , top pair production,  $W^+ Z^0 jj$ ,  $W^- Z^0 jj$ ,  $WZ$  production). The cross sections are shown in parenthesis. For the signal, we show the cross sections which give  $S/\sqrt{B} \simeq 3$  for  $|F|^2 = 1$ .

- Lepton cuts:

Three leptons with  $P_T > 30$  GeV and no other lepton with  $P_T > 20$  GeV.

By defining two leptons whose combination minimizes the quantity  $M_{\ell_i \ell_j} - m_Z$  ( $i, j = 1 - 3$ ,  $m_Z$  is the mass of the  $Z$  boson.) as  $\ell_{Z_1}$  and  $\ell_{Z_2}$ ,

$$\Delta R_{\ell_{Z_1} \ell_{Z_2}} < 1.0 \text{ for } m_{H^\pm} = 800 \text{ GeV,}$$

$$80 \text{ GeV} < M_{\ell_{Z_1} \ell_{Z_2}} < 100 \text{ GeV,}$$

$$170 \text{ GeV} < M_{\ell\ell\nu} < 240 \text{ GeV for } m_{H^\pm} = 200 \text{ GeV,}$$

$$450 \text{ GeV} < M_{\ell\ell\nu} < 600 \text{ GeV for } m_{H^\pm} = 500 \text{ GeV.}$$

	signal	backgrounds	
		$W + 4j$	$t\bar{t}$
Before cuts	100% (130 fb)	100% (130 pb)	100% (490 pb)
+Forward jet tagging	40% (52 fb)	50% (65 pb)	3.6% (18 pb)
+ $b$ -jet cuts	33% (43 fb)	47% (61 pb)	0.25% (1.2 pb)
+Lepton cuts	2.0% (2.6 fb)	2.0% (2.6 pb)	0.012% (0.059 pb)
+Central jet veto	0.62% (0.81 fb)	0.32% (0.42 pb)	0.0033% (0.016 pb)
+Central jet cuts	0.19% (0.25 fb)	0.0027% (3.5 fb)	0.0001% (0.49 fb)

	backgrounds		
	$W^+Z^0jj$	$W^-Z^0jj$	$WZ$
Before cuts	100% (350 fb)	100% (210 fb)	100% (26 pb)
+Forward jet tagging	43% (150 fb)	36% (76 fb)	1.1% (0.29 pb)
+ $b$ -jet cuts	37% (130 fb)	30% (63 fb)	0.99% (0.26 pb)
+Lepton cuts	1.5% (5.3 fb)	1.2% (2.5 fb)	0.015% (0.0039 pb)
+Central jet veto	0.40% (1.4 fb)	0.30% (0.63 fb)	0.0031% (0.81 fb)
+Central jet cuts	0.018% (0.063 fb)	0.022% (0.046 fb)	0.0001% (0.026 fb)

TABLE IV: Efficiencies and backgrounds for the signal ( $H^\pm \rightarrow W^\pm Z^0 \rightarrow jj\ell\nu$  decay modes at  $m_H^\pm = 500$  GeV) and backgrounds ( $W + 4j$ , top pair production,  $W^+Z^0jj$ ,  $W^-Z^0jj$ ,  $WZ$  production). The cross sections are shown in parenthesis. For the signal, we show the cross sections which give  $S/\sqrt{B} \simeq 3$  with  $|F|^2 = 1$ .

Since the cross section for the  $W^+Z^0jj$  production (the  $W^-Z^0jj$  production) is about 350 fb (210 fb), the signal cross sections of 170 fb, 89 fb and 54 fb are required to satisfy  $S/\sqrt{S+B} > 3$  for  $m_{H^\pm} = 200, 500$  and 800 GeV, respectively, under  $\mathcal{L} = 600 \text{ fb}^{-1}$ .

	signal		backgrounds	
			$W + 4j$	$t\bar{t}$
Before cuts	100%	(48 fb)	100% (130 pb)	100% (490 pb)
+Forward jet tagging	46%	(22 fb)	50% (65 pb)	3.6% (18 pb)
+ $b$ -jet cuts	38%	(18 fb)	47% (61 pb)	0.25% (1.2 pb)
+Lepton cuts	2.5%	(1.2 fb)	2.0% (2.6 pb)	0.012% (0.059 pb)
+Central jet veto	0.88%	(0.42 fb)	0.32% (0.42 pb)	0.0033% (0.016 pb)
+Central jet cuts	0.42%	(0.2 fb)	0.0016% (2.1 fb)	0.0001% (0.49 fb)

	backgrounds			
	$W^+ Z^0 jj$	$W^- Z^0 jj$	$WZ$	
Before cuts	100%	(350 fb)	100% (210 fb)	100% (26 pb)
+Forward jet tagging	43%	(150 fb)	36% (76 fb)	1.1% (0.29 pb)
+ $b$ -jet cuts	37%	(130 fb)	30% (63 fb)	0.99% (0.26 pb)
+Lepton cuts	1.5%	(5.3 fb)	1.2% (2.5 fb)	0.015% (0.0039 pb)
+Central jet veto	0.40%	(1.4 fb)	0.30% (0.63 fb)	0.0031% (0.81 fb)
+Central jet cuts	0.014%	(0.049 fb)	0.018% (0.038 fb)	0.0001% (0.026 fb)

TABLE V: Efficiencies and backgrounds for the signal ( $H^\pm \rightarrow W^\pm Z^0 \rightarrow jj\ell\nu$  decay modes at  $m_H^\pm = 800$  GeV) and backgrounds ( $W + 4j$ , top pair production,  $W^+ Z^0 jj$ ,  $W^- Z^0 jj$ ,  $WZ$  production) for . The cross sections are shown in parenthesis. For the signal, we show the cross sections which give  $S/\sqrt{B} \simeq 3$  for  $|F|^2 = 1$ .

### III. DISCUSSIONS

#### A. Possible values of the $H^\pm W^\mp Z^0$ vertex in several models

We here shortly summarize typical values of the form factor  $F$  in several new physics models[16]; i.e., two-Higgs doublet models (THDMs)(including the minimal supersymmetric standard model (MSSM))[12, 13, 14, 15, 26, 27, 28, 31], the littlest Higgs model[8, 9], and the model with a real and a complex triplet fields[3, 4, 5].

	signal		backgrounds					
			$W^+Z^0jj$	$W^-Z^0jj$	$WZ$			
Before cuts	100%	(170 fb)	100%	(350 fb)	100%	(210 fb)	100%	(26 pb)
+Forward jet tagging	31%	(53 fb)	43%	(150 fb)	36%	(76 fb)	1.1%	(0.29 pb)
+Lepton cuts	0.017%	(0.029 fb)	0.0040%	(0.014 fb)	0.0040%	(0.0084 fb)	(< 0.0026 fb)	

TABLE VI: Efficiencies and cross sections for the signal ( $H^\pm \rightarrow W^\pm Z^0 \rightarrow \ell\ell\nu$  decay modes at  $m_H^\pm = 200$  GeV) and backgrounds ( $W^+Z^0jj$ ,  $W^-Z^0jj$ ,  $WZ$  production). The cross sections are shown in parenthesis. For the signal, we show the cross sections which give  $S/\sqrt{S+B} \simeq 3$  for  $|F|^2 = 1$ .

	signal		backgrounds					
			$W^+Z^0jj$	$W^-Z^0jj$	$WZ$			
Before cuts	100%	(89 fb)	100%	(350 fb)	100%	(210 fb)	100%	(26 pb)
+Forward jet tagging	40%	(36 fb)	43%	(150 fb)	36%	(76 fb)	1.1%	(0.29 pb)
+Lepton cuts	0.030%	(0.027 fb)	0.0040%	(0.014 fb)	(< 0.0042 fb)		(< 0.0026 fb)	

TABLE VII: Efficiencies and cross sections for the signal ( $H^\pm \rightarrow W^\pm Z^0 \rightarrow \ell\ell\nu$  decay modes at  $m_H^\pm = 500$  GeV) and backgrounds ( $W^+Z^0jj$ ,  $W^-Z^0jj$ ,  $WZ$  production). The cross sections are shown in parenthesis. For the signal, we show the cross sections which give  $S/\sqrt{S+B} \simeq 3$  for  $|F|^2 = 1$ .

In the THDM<sup>2</sup>, there are two sources to enhance the loop-induced form factors; i.e., the contribution from the top-bottom loop and those from the Higgs-boson loop. The values of  $F^{(t-b \text{ loop})}$  are given by  $F^{(t-b \text{ loop})} \simeq 0.01 \cot \beta$ ; i.e.,  $|F^{(t-b \text{ loop})}|^2 \simeq 10^{-3}, 10^{-4}$  and  $10^{-5}$  for  $\tan \beta = 0.3, 1$  and  $3$ , respectively, where  $\tan \beta$  is the ratio of vacuum expectation values for neutral components of the two Higgs doublets. The contribution of the Higgs boson loop can be important for  $\tan \beta \gtrsim 3$ , where the top-bottom loop contribution becomes suppressed because of the smaller Yukawa couplings[26]. The Higgs loop effect on  $F$  is constrained from perturbative unitarity[29, 30] as  $|F^{(\text{bosonic loop})}|^2 \lesssim 10^{-5}$  for  $3 \lesssim \tan \beta \lesssim 10$ . Therefore, the

<sup>2</sup> We consider Model II THDM[2].

	signal		backgrounds					
			$W^+Z^0jj$		$W^-Z^0jj$		$WZ$	
Before cuts	100%	(54 fb)	100%	(350 fb)	100%	(210 fb)	100%	(26 pb)
+Forward jet tagging	46%	(25 fb)	43%	(150 fb)	36%	(76 fb)	1.1%	(0.29 pb)
+Lepton cuts	0.090%	(0.049 fb)	0.026%	(0.091 fb)	0.010%	(0.021 fb)	(< 0.0026 fb)	

TABLE VIII: Efficiencies and cross sections for the signal ( $H^\pm \rightarrow W^\pm Z^0 \rightarrow \ell\ell\nu$  decay modes at  $m_H^\pm = 800$  GeV) and backgrounds ( $W^+Z^0jj$ ,  $W^-Z^0jj$ ,  $WZ$  production). The cross sections are shown in parenthesis. For the signal, we show the cross sections which give  $S/\sqrt{S+B} \simeq 3$  for  $|F|^2 = 1$ .

value of  $|F^{(\text{THDM})}|^2$  can be at most  $\sim 10^{-3}$ ,  $10^{-4}$  and  $10^{-5}$  for  $\tan\beta = 0.3$ , 1 and 3 – 10, respectively. In the MSSM, the loop effect of super partner particles can enhance the vertex especially in the moderate values of  $\tan\beta$ . However, its magnitude is not large and at most less than  $10^{-5}$ [31] for  $\tan\beta \gtrsim 3$ .

In models with triplets, the  $H^\pm W^\mp Z^0$  vertex generally appears at the tree level. A common feature of the tree level contribution to the form factor  $F$  is the fact that it is proportional to the vacuum expectation values (VEVs) of the triplet field[2, 3],  $F \propto v'/v$ , where  $v$  and  $v'$  represent the VEVs of the doublet and the triplet in the model, respectively. When more than one triplet appear in the model,  $v'$  should be taken as the combination of the VEVs for them. In the Littlest Higgs model, an additional complex triplet field appears in the effective theory. The electroweak data indicate  $1 \lesssim v' \lesssim 4$  GeV for  $f = 2$  TeV[32]. We here consider the case with  $m_h = 115$  GeV,  $f = 1$  TeV (2 TeV),  $v' = 5$  GeV (4 GeV), and  $m_{H^\pm} = 700$  GeV (1.56 TeV) as a reference: i.e., the value of the form factor  $F$  is  $|F^{(\text{LLH})}|^2 \simeq 0.0085$  (0.0054).

In the model with additional real and complex triplet fields, the rho parameter can be set to be unity at the tree level, by imposing the custodial symmetry; i.e.,  $v'_r = v'_c (= v')$ , where  $v'_r$  and  $v'_c$  are respectively the VEVs of the real and the complex triplet field[3, 4, 5]. The strongest experimental bound on  $v'/v$  comes from the  $Zb\bar{b}$  result. The limits at 95% CL are  $\tan\theta_H \lesssim 0.5, 1$  and 1.7 for the mass of  $H_3$  to be 0.1, 0.5 and 1 TeV, respectively[6]. We here take  $\tan\theta_H$  to be 0.5 where  $\sin\theta_H = \sqrt{8v'^2/(v^2 + 8v'^2)}$  and  $m_{H^\pm}$  to be 200 GeV;

i.e.,  $|F^{(\text{triplet})}|^2 \simeq 0.26$ . For greater values of  $m_{H^\pm}$ , the constraint is relaxed.

## B. Feasibility

The decay pattern of  $H^\pm$  depends on the model.

### 1. $H^\pm \rightarrow t\bar{b}$ ( $\bar{t}b$ )

In the THDM and the MSSM, although there are potentially many decay modes, the main mode would be the decay into a  $tb$  pair as long as it is kinematically allowed. The main decay mode of the Littlest Higgs model would also be the decay into a  $tb$  pair[9]. In these cases, the signal can be a  $bb\ell\nu$  ( $\ell = e$  and  $\mu$ ) event. As shown in Sec. II, the required cross section to satisfy  $S/\sqrt{B} \gtrsim 3$  after background reduction is  $\sigma_S \gtrsim 160$  fb (22 fb) for  $m_{H^\pm} = 200$  GeV (700 GeV), which corresponds to  $|F|^2 \gtrsim 0.041$  ( $|F|^2 \gtrsim 0.10$ ), where  $\sigma_S$  is the signal cross section before kinematical cuts. Hence, the typical values of  $|F|^2$  in the THDM, the MSSM and the littlest Higgs model are all smaller than the required one for  $S/\sqrt{B} \gtrsim 3$ <sup>3</sup>. The branching ratio of  $H^\pm \rightarrow t\bar{b}$  ( $\bar{t}b$  is assumed to be 100%). Therefore, we must conclude that testing these models through this process is challenging.

### 2. $H^\pm \rightarrow W^\pm Z^0$

In models with triplets that do not couple to fermions, it would mainly decay into a  $WZ$  pair. The model with a real and a complex triplets can correspond to this case. The signal event can be  $jj\ell\nu$  and  $\ell\ell\ell\nu$ . See Sec II.

For the  $jj\ell\nu$  event, the required values of the production cross section to satisfy the statistical significance  $S/\sqrt{B} \gtrsim 3$  after background reduction is  $\sigma_S \gtrsim 870, 130$  and  $48$  fb for  $m_{H^\pm} = 200, 500$  and  $800$  GeV, respectively. The corresponding values of  $|F|^2$  are  $|F|^2 \gtrsim 0.23, 0.28$  and  $0.32$ . For the  $\ell\ell\ell\nu$  event, the required values of the production cross section to satisfy the statistical significance  $S/\sqrt{S+B} \gtrsim 3$  after background reduction is

---

<sup>3</sup> When the variation of the models such as the littlest Higgs model with only gauging the SM  $U(1)_Y$  subgroup [33] are considered, the  $F$  values can be larger. Then, the observation may be possible

$m_H^\pm$ (GeV)	200	700
$ F ^2$ for $bb\nu$	0.041	0.10

TABLE IX: Required  $|F|^2$  values for  $S/\sqrt{B} \sim 3$  for the  $H^\pm \rightarrow t\bar{b}(\bar{t}b) \rightarrow bbl\nu$  decay mode at  $\mathcal{L} = 600 \text{ fb}^{-1}$ .

$m_H^\pm$ (GeV)	200	500	800
$ F ^2$ for $jj\nu$	0.23	0.28	0.32
$ F ^2$ for $ll\nu$	0.044	0.19	0.36

TABLE X: Required  $|F|^2$  values for  $S/\sqrt{B} \sim 3$  for the  $H^\pm \rightarrow W^\pm Z^0 \rightarrow jj\nu$  and  $ll\nu$  decay modes at  $\mathcal{L} = 600 \text{ fb}^{-1}$ .

$\sigma_S \gtrsim 170, 89$  and  $54 \text{ fb}$  for  $m_{H^\pm} = 200, 500$  and  $800 \text{ GeV}$ , respectively. The corresponding values of  $|F|^2$  are  $|F|^2 \gtrsim 0.044, 0.19$  and  $0.36$ . The results are similar to those in Ref. [34].

Therefore, this model can be tested via the process of the  $H^\pm$  production via  $WZ$  fusion with the decay mode of  $H^\pm \rightarrow W^\pm Z^0$  at the LHC.

#### IV. CONCLUSIONS

The  $H^\pm W^\mp Z^0$  vertex strongly depends on the structure of the Higgs sector in various new physics scenarios, so that its measurement can be useful to distinguish the models. In this paper, the possibility of measuring this vertex has been studied by using the single  $H^\pm$  production via  $WZ$  fusion at the CERN Large Hadron Collider. A signal and background simulation under the expected detector performance at LHC is performed. Required values of  $|F|^2$  for  $S/\sqrt{B} \gtrsim 3$  are obtained for the decay modes of  $H^\pm \rightarrow t\bar{b}(\bar{t}b)$  and  $H^\pm \rightarrow W^\pm Z^0$  :see Tables IX and X, respectively.

The decay mode of  $H^\pm \rightarrow t\bar{b}(\bar{t}b) \rightarrow bbl\nu$  can be used to test  $H^\pm W^\mp Z^0$  vertex in multi-Higgs doublet models, the MSSM as well as the littlest Higgs model. However, the required magnitude of the form factor  $F$  for the observation at the LHC is turned out to be above the predicted maximal values of  $|F|^2$  in these models. The maximal value of  $|F|^2$  in the 2HDM is less by 2 orders than the required magnitude of  $|F|^2$ , and in the littlest Higgs model the

predicted  $|F|^2$  values are less than the required  $|F|^2$  value by 1 order. If we go to the SLHC, the 10 times larger luminosity may be expected. However, it is not easy to observe because the  $b$  tagging efficiency should be much worse than that of the LHC. On the other hand, it turns out that the process with the decay  $H^\pm \rightarrow W^\pm Z^0 \rightarrow \ell\ell\nu$  and  $jj\ell\nu$  can be useful to test the model with a real and a complex triplet fields.

### *Acknowledgments*

The authors would like to thank Shoji Asai, Tomio Kobayashi and Mihoko Nojiri for useful discussions. A part of this work started in the discussion during the workshop ‘‘Physics in LHC era’’ at YITP, 13-15 December 2004 (YITP-W-04-20). S.K. was supported, in part, by Grants-in-Aid of the Ministry of Education, Culture, Sports, Science and Technology, Government of Japan, Grant Nos. 17043008 and 18034004.

- 
- [1] ATLAS Collaboration, *Detector and Physics Performance Technical Design Report*, CERN/LHCC/99-14 (1999); CMS Collaboration, *CMS Technical proposal*, CERN/LHCC 94-38, CERN (1994).
  - [2] J.F. Gunion, et al., *The Higgs Hunter’s Guide*, Addison-Wesley, New York, 1990.
  - [3] P. Galison, Nucl. Phys. B 232 (1984) 26; H. Georgi, M. Machacek, Nucl. Phys. B 262 (1985) 463; R. Chivukura, H. Georgi, Phys. Lett. B 182 (1986) 181.
  - [4] M. Chanowitz, M. Golden, Phys. Lett. B 165 (1985) 105.
  - [5] J. Gunion, R. Vega, J. Wudka, Phys. Rev. D 42 (1990) 1673; Phys. Rev. D 43 (1991) 2322.
  - [6] H. Haber, H. Logan, Phys. Rev. D 62 (2000) 015011.
  - [7] J.C. Pati, A. Salam, Phys. Rev. D 10 (1974) 275; R.N. Mohapatra, J.C. Pati, Phys. Rev. D 11 (1975) 2558; G. Senjanovic, R.N. Mohapatra, Phys. Rev. D 12 (1975) 1502.
  - [8] N. Arkani-Hamed, et al., J. High Energy Phys. 07 (2002) 034.
  - [9] T. Han, et al., Phys. Rev. D 67 (2003) 095004.
  - [10] N. Arkani-Hamed, S. Dimopoulos, Phys. Rev. D 65 (2002) 052003; N. Arkani-Hamed, et al., Phys. Rev. D 61 (2000) 116003; E. Ma, U. Sarkar, Phys. Rev. Lett. 80 (1998) 5716.
  - [11] J.A. Grifols, A. Méndez, Phys. Rev. D 22 (1980) 1725; A.A. Iogansen, N.G. Uraltsev, V.A. Khoze, Sov. J. Nucl. Phys. 36 (1982) 717.

- [12] T.G. Rizzo, *Mod. Phys. Lett. A* 4 (1989) 2757; A. Méndez, A. Pomarol, *Nucl. Phys. B* 349 (1991) 369; J.L. Díaz-Cruz, J. Hernández-Sánchez, J.J. Toscano, *Phys. Lett. B* 512 (2001) 339.
- [13] M. Capdequi Peyranère, H.E. Haber, P. Irulegui, *Phys. Rev. D* 44 (1991) 191.
- [14] S. Kanemura, *Phys. Rev. D* 61 (2000) 095001.
- [15] A. Arhrib, R. Benbrik, M. Chabab, hep-ph/0607182.
- [16] E. Asakawa, S. Kanemura, *Phys. Lett. B* 626 (2005) 111.
- [17] R.N. Cahn et al., *Phys. Rev. D* 35 (1987) 1626; V.D. Barger, T. Han, R.J.N. Phillips, *Phys. Rev. D* 37 (1988) 2005; R. Kleiss, W.J. Stirling, *Phys. Lett. B* 200 (1988) 193; U. Baur, E.W.N. Glover, *Nucl. Phys. B* 347 (1990) 12; U. Baur, E.W.N. Glover, *Phys. Lett. B* 252 (1990) 683; V. Barger et al., *Phys. Rev. D* 44 (1991) 1426.
- [18] D. Rainwater, D. Zeppenfeld, *J. High Energy Phys.* 12 (1997) 005; D. Rainwater, D. Zeppenfeld, K. Hagiwara, *Phys. Rev. D* 59 (1999) 014037; T. Plehn, D. Rainwater, D. Zeppenfeld, *Phys. Rev. D* 61 (2000) 093005; T. Plehn, D. Rainwater, D. Zeppenfeld, *Phys. Rev. Lett.* 88 (2002) 051801; N. Kauer et al., *Phys. Lett. B* 503 (2001) 113; T. Plehn, D. Rainwater, *Phys. Lett. B* 520 (2001) 108.
- [19] D. Rainwater and D. Zeppenfeld, *Phys. Rev. D* 60 (1999) 113004.
- [20] S. Asai, et al., *Eur. Phys. J. C* 32S2 (2004) 19.
- [21] T. Sjöstrand, *Comp. Phys. Comm.* 82 (1994).
- [22] H.L. Lai, et al., *EPJC* 12 (2000) 375.
- [23] T. Stelzer, W.F. Long, *Comp.Phys. Comm.* 81, 357 (1994); F. Maltoni, T. Stelzer, *J. High Energy Phys.* 0302 (2003) 027.
- [24] S. Kretzer, et al., *Phys. Rev. D* 69 (2004) 114005.
- [25] E. Richter-Was, D. Froidevaux, L. Poggioli, *ATLFAST 2.0, a fast simulation package for ATLAS*, ATLAS internal note ATL-PHYS-98-131 (1998).
- [26] S. Kanemura, *Eur. Phys. J. C* 17 (2000) 473.
- [27] S.-H. Zhu, hep-ph/9901221; A. Arhrib, et al., *Nucl. Phys. B* 581 (2000) 34.
- [28] S. Kanemura, S. Moretti, K. Odagiri, *J. High Energy Phys.* 02 (2001) 011.
- [29] B.W. Lee, C. Quigg, H.B. Thacker, *Phys. Rev. D* 16 (1977) 1519.
- [30] H. Hüffel, G. Pocsik, *Z. Phys. C* 8 (1981) 13; J. Maalampi, J. Sirkka, I. Vilja, *Phys. Lett. B* 265 (1991) 371; S. Kanemura, T. Kubota, E. Takasugi, *Phys. Lett. B* 313 (1993) 155;

- A. Akeroyd, A. Arhrib, E.-M. Naimi, Phys. Lett. B 490 (2000) 119; I.F. Ginzburg, I.P. Ivanov, hep-ph/0312374.
- [31] H.E. Logan, S. Su, Phys. Rev. D 66 (2002) 035001; Phys. Rev. D 67 (2003) 017703.
- [32] M.-C. Chen, S. Dawson, Phys. Rev. D 70 (2004) 015003.
- [33] C. Csaki et al., Phys. Rev. D 68 (2003) 035009.
- [34] A. Birkedal, K. Matchev, M. Perelstein, Phys. Rev. Lett. 94 (2005) 191803.